JOURNAL OF BONE AND MINERAL RESEARCH
Volume 17, Number 6, 2002
© 2002 American Society for Bone and Mineral Research

Mineralization of Developing Mouse Calvaria as Revealed by Raman Microspectroscopy

CATHERINE P. TARNOWSKI,[1] MICHAEL A. IGNELZI JR.,[2] and MICHAEL D. MORRIS[1]

ABSTRACT

Raman microspectroscopy is a nondestructive vibrational spectroscopic technique that permits the study of organic and mineral species at micron resolution, offers the ability to work with hydrated and dehydrated specimens in vivo or in vitro, and requires minimal specimen preparation. We used Raman microspectroscopy to determine the composition of the mineral environments present in mouse calvaria, the flat bones that comprise the top of the skull. We have acquired Raman transects (lines of point spectra) from mouse calvaria during a developmental time course ranging from embryonic day 13.5 (E13.5; 6 days before birth) to 6 months of age. Exploratory factor analysis (FA) reveals the presence of a variety of apatitic mineral environments throughout the tissue series. The earliest mineral is observed in the fetal day 15.5 (F15.5) mice and is identified as a carbonated apatite. The presence of a heterogeneous mineralized tissue in the postnatal specimens suggests that ionic incorporation and crystal perfection in the lattice vary as the mouse develops. This variation is indicative of the presence of both recently deposited mineral and more matured remodeled mineral. Band area ratios reveal that the mineral/matrix ratio initially increases, reaches a plateau, and then increases again. The carbonate/phosphate band area ratio remains constant from F18.5 to postnatal day 3 (PN3) and then increases with age. Insights into the chemical species, the degree of mineralization, and the multiple mineral environments that are present in normal calvarial tissue will enable us to better understand both normal and abnormal mineralization processes. (J Bone Miner Res 2002;17:1118–1126)

Key words: Raman spectroscopy, mineralization, bone, mouse, calvaria

INTRODUCTION

Identifying the composition of the mineral and matrix environments in early mineralized tissue is crucial to understanding the initial mineralization process. It is well known that the mineral lattice formed during early stages of development of the calvaria (the flat bones that comprise the skull), as in the mandible and other skeletal elements, occurs through intramembranous ossification (IO); however, the composition of the initial mineral deposited *in vivo* is unknown. It is recognized that IO is mediated through osteoblast-derived cells rather than the cartilage-mediated deposition that characterizes endochondral ossification. These osteoblast-derived cells sequester the calcium and phosphate needed to form the initial mineral lattice, which then is deposited onto a collagen matrix. Needle-like crystalline structures have been observed in these osteoblastic cells both in cell cultures[(1)] and in sectioned rat calvaria.[(2)] Stanford and colleagues found that the initial mineral crystals formed in the osteoblastic cell cultures have X-ray diffraction (XRD) patterns that resemble those of substituted apatites found in mature bone tissue.[(1)] Recently, Kuhn and coworkers also have studied the mineral crystallites found in embryonic chick cell cultures using Fourier-

The authors have no conflict of interest.

[1]Department of Chemistry, University of Michigan, Ann Arbor, Michigan, USA.
[2]Department of Orthodontics and Pediatric Dentistry, University of Michigan School of Dentistry, Ann Arbor, Michigan, USA.

TABLE 1. BAND ASSIGNMENTS FOR RAMAN SPECTRA OF TISSUE

Raman frequency shift (cm^{-1})	*Assignment (intensity)*
580	PO_4^{3-} ν_4, (m)[a]
855	Proline ring (w)
876	Hydroxyproline ring (w)
950–964	PO_4^{3-} ν_1 (P—O symmetric stretch; vs)[a]
1001–1003	Ring breathing mode of phenlyalanine (m)
1030	PO_4^{3-} ν_3 (P—O asymmetric stretch; m)[a]
1065–1070	CO_3^{2-} ν_1 (C—O in plane stretch; m)[a]
1245, 1270	Amide III, C—N—H stretch (m)
1445	CH_2 wag (m)
1665	Amide I, C—C—N stretch (m)

[a] Denotes a mineral band.
vs, very strong; m, medium; w, weak.

transform infrared (FTIR) spectroscopy.[3] The earliest mineral crystallite, found in 8-day-old cultures, consisted of a carbonated apatite with the presence of monohydrogen phosphate (HPO_4^{2-}) ions. Kuhn and colleagues also found that the carbonate content in 60-day-old cell culture apatitic mineral increased from the amount found in the 8-day-old culture. Although both of these studies have characterized the earliest mineral environments found in their respective systems, both are studies of osteoblastic cell cultures rather than of mineralized tissue in vivo.

Alizarin red/Alcian blue staining has shown that the initial mineral deposition in mouse calvaria occurs at fetal day 15.5 (F15.5; 4 days before birth).[4] The shortcoming of alizarin red/Alcian blue staining is that it can determine only the presence of mineral; it is unable to characterize the species that constitute the deposited mineral lattice. Raman spectroscopy overcomes this limitation by using information from the vibrational spectra of the ions within a mineral lattice to identify the mineral formed in these early stages of bone development.

Raman vibrational spectroscopy has been used to study mineralized tissues and cell cultures.[5–13] Raman spectroscopy offers several technical advantages. It has excellent spatial resolution (capable of 0.5–1 μm) and, in general, the vibrational bands are narrow so that small frequency shifts and band shape changes often are observed easily. These narrow vibrational bands allow one to distinguish between various chemical species. When Raman spectroscopy is used, specimen preparation is simple; specimens need not be transparent or fixed. Hydrated or dehydrated specimens may be subjected to Raman spectroscopy and because Raman spectroscopy is nondestructive, the same developing tissue can be evaluated over a period of time.

In biological tissues, Raman spectroscopy probes the molecular and ionic vibrations of mineralized species such as phosphate, carbonate, and monohydrogen phosphate, as well as the many vibrations that arise from the proteinaceous matrix. In Raman spectra, the symmetrical vibrations of a molecule or ion are the most intense vibrational bands observed.[14,15] The major mineral and matrix bands in the Raman spectrum of bone tissue are summarized in Table 1.

The PO_4^{3-} symmetric stretch (ν_1), the most prominent vibrational band in the Raman spectrum of mineralized tissue, is critical to our understanding of the mineral environments present in the tissue. Advantageously, both the PO_4^{3-} symmetric stretch (ν_1) frequency and the band shape depend on the local mineral environment and therefore change with ionic incorporation and crystallinity. Many studies on apatitic tissue and synthetic apatitic lattices have correlated the PO_4^{3-} symmetric stretch (ν_1) band frequency with the mineral environment composition. In particular, hydroxyapatite, carbonate-substituted apatite, amorphous calcium phosphate, octacalcium phosphate, and dicalcium phosphate dihydrate all have characteristic PO_4^{3-} ν_1 frequencies.[12,16] In mineralized tissue Raman spectroscopy, it is useful to classify the apatitic environments using three broad categories with three different band frequencies. B-type carbonate-substituted apatite (carbonate substituted for phosphate in the hydroxyapatite lattice) produces a Raman-shifted frequency in the range of 955 cm^{-1}–959 cm^{-1}. In a crystalline nonsubstituted hydroxyapatite, the PO_4^{3-} ν_1 Raman-shifted frequency is found in the region of 962 cm^{-1}–964 cm^{-1}. Finally, a band with a Raman-shifted frequency in the 945 cm^{-1}–950 cm^{-1} is indicative of a disordered phosphate apatitic lattice. Whether this band frequency arises from A-type carbonate substitution (carbonate for hydroxide) or from an amorphous calcium phosphate is not clear; therefore, we prefer to use the term "disordered phosphate" to describe this mineral environment. Most bone tissue contains some amount of each of these three mineral environments; consequently, the resulting bone tissue phosphate ν_1 band is a sum of all three bands. Typically, the most prominent mineral environment identified throughout bone tissue is the carbonated apatitic phosphate. Hence, in a bone spectrum, the phosphate ν_1 band peak frequency usually is in the 955- to 959-cm^{-1} range. The phosphate ν_1 band often is asymmetric because of the addition of varying contributions from the disordered phosphate and the more crystalline nonsubstituted phosphate to the left and right sides of the main band, respectively. Variations in the phosphate ν_1 band shape and peak frequency can reveal changes in the mineral environment because of ionic incorporation or crystallinity at different stages of development and are important to our understanding of the mineralization processes.

We are able to monitor and resolve changes in the phosphate ν_1 band shape and frequency as well as the changes in the relative amounts of the rest of the tissue components using a multivariate analysis technique, factor analysis (FA). Although univariate analyses such as band area or intensity ratios may be more familiar and used more often in spectroscopic tissue analyses, multivariate analyses are well known in the fluorescence imaging and magnetic resonance imaging (MRI) communities[17,18] as well as in the chemistry community.[19,20] The advantages of using FA as an analysis tool is that it has an inherent signal-averaging effect and has the ability to resolve spectral components that are present in different proportions in a series of spectra. This is especially important for bone tissue, which can be very heterogeneous, resulting in considerable variation in its Raman spectra.

Essentially, a complete FA results in factors and scores; the greater the number of tissue factors, the greater the number of mineral and matrix environments. In our work, a factor is a descriptor of a tissue or background component and resembles a Raman spectrum. Each factor has a corresponding score; this score describes the relative amount of that factor (tissue component) present in each original spectrum of the transect. If two tissue components are found in different ratios throughout the specimen being probed, their spectral signatures will be separated into two factors. Their corresponding scores will reflect the variation throughout the specimen. For example, if the mineral and the collagen present in the tissue have a constant ratio throughout that tissue, FA will produce a factor in which the spectral signatures of the mineral and the collagen are combined. However, if the ratio of mineral to collagen varies throughout the tissue probed, the FA will separate the spectral signatures of the two species into two separate factors. These two factors also will have separate scores. Their individual scores will reveal where the relative amounts of mineral and collagen differ throughout the tissue probed. Therefore, FA is an excellent choice for detecting variations in the mineral and matrix environments throughout the tissue, because these variations are reflected in the original spectra as small changes in either the shape of the spectroscopic bands or in the band ratios of different tissue components. It is important to note that as the variation in the mineral and matrix environments in the tissue increases, there will be an increase in the number of tissue factors.

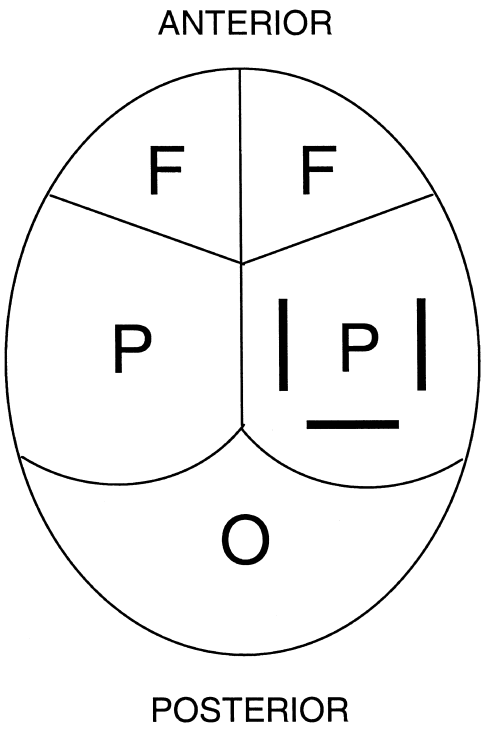

FIG. 1. Schematic diagram of the endocranial surface of the mouse calvaria: (F) frontal bone, (P) parietal bone, (O) occipital bone. Bold lines indicate the three general areas where Raman transects were acquired in each mouse.

MATERIALS AND METHODS

Specimen preparation

B6CBA F_1/J wild-type mice (The Jackson Laboratory, Bar Harbor, ME, USA) were harvested at nine different developmental time points: embryonic days 13.5 (E13.5) and E14.5; F15.5 and F18.5; postnatal days 1 (PN1), PN3, PN7, and PN14; and postnatal 6 months. The flat bones of the top-most portion of the skull, the calvaria, were removed intact and rinsed of debris using phosphate-buffered saline (PBS) at pH 7.2. Then, the tissue was fixed in 100% ethanol for 30–60 minutes, soaked in 95% ethanol for 20 minutes, and transferred to 70% ethanol for storage at 4°C. Before the spectroscopic experiments, the specimens were soaked in PBS to avoid dehydration during spectral acquisition. The calvarial specimens were placed between a quartz slide and coverslip (Esco Products, Inc., Oak Ridge, NJ, USA) for the duration of the experiment.

Raman spectroscopy

The method by which the Raman spectra were obtained and the instrument design have been described previously.[8] Briefly, a 785-nm diode laser (80 mW at specimen; SDL, Inc., San Jose, CA, USA) was focused onto the specimens using a 10X/0.5 NA objective (Fluar Series; Zeiss, Thornwood, NY, USA) mounted on a BH-2 microscope frame (Olympus, Inc., Melville, NY, USA). In the epi-illumination configuration, the Raman scatter was collected by the same objective and focused into an NIR-optimized spectrograph (HoloSpec f/1.8I; Kaiser Optical Systems, Inc., Ann Arbor, MI, USA). The spectrograph dispersed the Raman scatter onto a liquid-nitrogen cooled camera (MASD; Roper Scientific, San Diego, CA, USA). A 25-μm entrance slit was used to set the spectral resolution of the system to 3–4 cm^{-1}. A motorized translation stage (New England Affiliated Technologies, Danaher Precision Systems, Salem, NH, USA) moved the specimen at 2-μm increments under the focused laser spot to provide a 4-μm spatial resolution.

Six Raman transects (lines of point spectra) were acquired for each developmental time point. For F18.5 and each postnatal time point, two mice were examined in three different areas on the endocranial surface of the parietal bone. One transect was acquired along the edge nearest to the occipital bone, one transect was acquired laterally, and one transect was acquired adjacent to the sagittal suture (Fig. 1, bold lines). Because there was significantly less mineral in the F15.5 mice, only one area on the endocranial surface of the parietal bone was examined per mouse; six mice were examined for this time point. All Raman transects were acquired with a 4-μm spatial resolution and ranged in length from 200 to 250 μm.

Data analysis

All data analysis was performed using MatLab 5.3 (MathWorks, Inc., Natick, MA, USA) using vendor-supplied and

locally written scripts. All spectra were preprocessed by removing detector-generated artifacts (spikes) and subtracting the detector dark current.

FA identifies tissue components, as does the examination of raw spectra, but FA also reveals how various tissue components change over time with relation to one another. FA was performed on the data by calculating the covariance matrix (the data set matrix multiplied by its transpose) of the transect spectra data set[20] and then carrying out a principal component analysis, which enhances any small changes in the Raman spectra throughout the data set. This principal component analysis results in set of eigenvectors that describes the original data set. Most of these eigenvectors describe noise in the system; these noise-describing eigenvectors are discarded. The rest of the nonnoise eigenvectors are rotated manually (added and subtracted from one another), resulting in "factors." These factors describe the original spectral signatures of the various tissue components. Nonnegativity and band shapes were used as rotational constraints.[21]

Before any univariate analysis, any spectrum without a signal-to-noise ratio >3 in the PO_4^{3-} ν_1 envelope (920–980 cm^{-1}) was identified as a nonmineral spectrum and thus discarded. Using this criterion, some spectra were discarded only from F15.5 and 18.5 transects—the transects with the least mineral deposition. Before band area calculations, a linear baseline was subtracted from each band envelope and the band was then offset to zero. The procedures used to obtain the carbonate/phosphate and mineral/matrix ratios are similar to those used by Camacho et al. in their analysis of FTIR human bone tissue spectra.[22]

The carbonate/phosphate ratios for each transect were calculated from an average of the carbonate/phosphate band area ratios from three spectra. Only three spectra were chosen for carbonate/phosphate analysis because in some of the transect spectra, there was less mineral signal present and as a result, the signal to noise ratio in the carbonate envelope was not large enough to determine reliably the carbonate band area. The three spectra chosen for carbonate/phosphate analysis contained a strong mineral signal (determined by the mineral scores from the FA) and were spaced widely throughout the data set so as to include any variation in the tissue's mineral environments. Two or three bands (~1030 cm^{-1} PO_4^{3-} ν_3, ~1045 cm^{-1} PO_4^{3-} ν_3, and ~1070 cm^{-1} CO_3^{2-} ν_1) were fit to the baseline-corrected PO_4^{3-} ν_3, CO_3^{2-} ν_1 envelope (1015–1090 cm^{-1}). The area of the 1070-cm^{-1} band only was used as a metric for the carbonate content. The integrated area of the baseline-corrected PO_4^{3-} ν_1 envelope (920–980 cm^{-1}) was used as a measure of the phosphate content. A global average carbonate/phosphate ratio for each time point was obtained by averaging the mean carbonate/phosphate ratio from each of the six transects for each time point.

The area of the baseline-corrected PO_4^{3-} ν_1 envelope (920–980 cm^{-1}) discussed previously was used as a measure of the mineral content in the mineral/matrix ratio. The area of the baseline-corrected amide I band envelope (1600–1720 cm^{-1}) was calculated and used as a measure of the matrix content. The mineral/matrix ratios were calculated for each spectrum of a transect and averaged. This mean mineral/matrix ratio for each transect was used to find the global average mineral/matrix ratio for each time point.

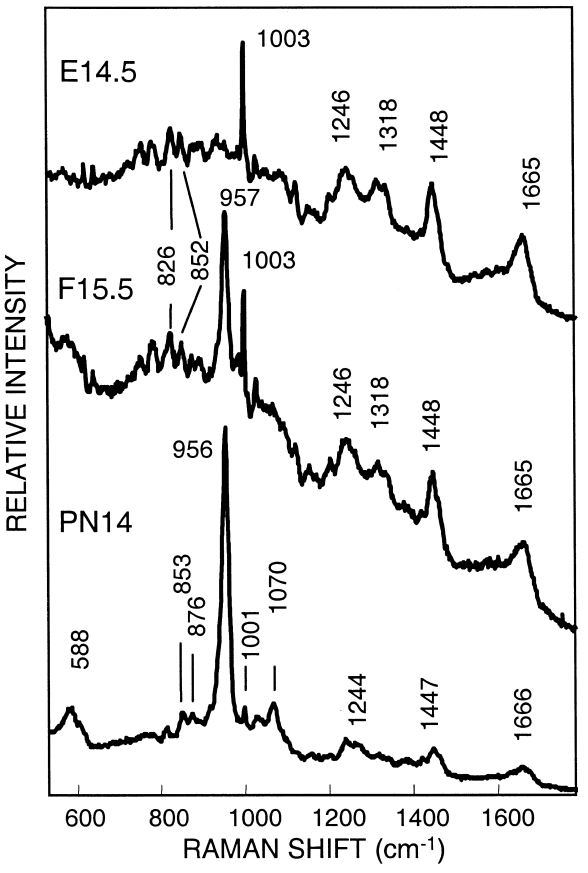

FIG. 2. Raman spectra reveal first signs of mineral at F15.5. Selected Raman spectra from three specimens: E14.5, F15.5, and PN14. Spectra are offset for clarity. The 785-nm excitation (80 mW) focused onto specimens through a 10×/0.50 NA objective. There is no detectable phosphate ν_1 band (957 cm^{-1}) in the E14.5 spectrum, although it is prominent in the F15.5 and PN14 spectra. The band area and intensity ratios of the phosphate (957 cm^{-1}) to the collagen-dominated protein (1003 cm^{-1} or 1665 cm^{-1}), a reflection of mineral/matrix ratio, increase with age from F15.5 to PN14.

RESULTS

Raman spectra

Selected Raman spectra from E14.5, F15.5, and PN14 transects are shown in Fig. 2. The embryonic spectrum (E14.5) contains only a collagen-dominated protein signature, suggesting that no mineral has been formed at this stage in the areas probed by Raman spectroscopy. This first sign of mineral appears at F15.5 in the form of an apatitic phosphate (956–957 cm^{-1}). This same apatitic phosphate band is seen at PN14. Both F15.5 and PN14 also contain the protein signature similar to the one found at E14.5. The relative intensity ratio of the phosphate ν_1 (956–957 cm^{-1}) band to that of the primarily collagen-dominated matrix bands (either 1003 cm^{-1} or the 1665-cm^{-1} band) in the two

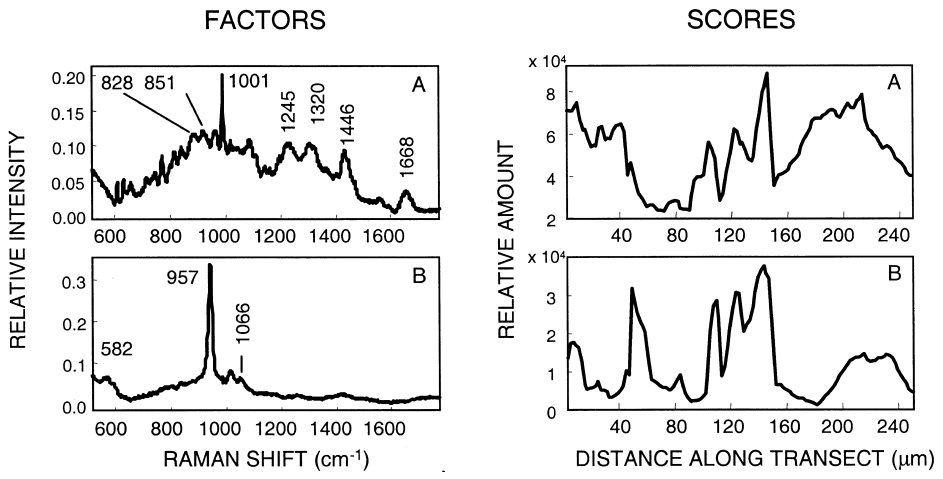

FIG. 3. FA reveals the presence of only one resolvable mineral species at F15.5. Factors describe specific chemical species in the tissue; scores describe the relative amount of each factor at a given location in the tissue probed. Areas where one score varies from another denote variation in the tissue environment. The 785-nm excitation (80 mW) focused onto specimens through a 10×/0.50 NA objective, spectra acquired at 2-μm increments. Data were acquired from the endocranial side of the parietal bone. Mineral subregion factors and scores from an F15.5 specimen. Factor A, collagen-dominated protein; factor B, carbonated apatitic mineral (PO_4^{3-} ν_1, 957 cm^{-1}; CO_3^{2-} ν_1, 1066 cm^{-1}). Four nontissue factors (two featureless backgrounds, buffer, and quartz) have been omitted for clarity.

spectra with mineral increases dramatically with age (Fig. 2, F15.5 and PN14), indicating that an increased amount of the mineral is found in the older tissue.

Multivariate data analysis

FA: The FA results from the individual transects can be used to sort the different aged mice into four distinct groups. The first group contains tissue with no mineral (E13.5 and E14.5). The second group contains tissue with only one mineral factor (F15.5 and F18.5). The third (PN1 and PN3) and fourth (PN7 and PN14 and postnatal 6 months) groups contained tissues with three and two resolvable mineral factors, respectively. As mentioned previously, the greater the number of resolvable tissue factors (descriptors), the greater the variation throughout the tissue.

E13.5 and E14.5. Transects from E13.5 and E14.5 calvaria were found to contain only a collagen-dominated protein. There was no detectable presence of any phosphate mineral.

F15.5 and F18.5. F15.5 and F18.5 calvarial transects all contained only one mineral factor, an apatitic phosphate lattice with a small amount of B-type carbonation (PO_4^{3-} ν_1, 957 cm^{-1}; CO_3^{2-} ν_1, 1066 cm^{-1}). Figure 3 presents the factors and scores from an F15.5 transect (four nontissue factors were omitted for clarity). Each factor describes a tissue component found in the specimen. Its corresponding score describes the relative amount of that component found in the original data set. For instance, there is more signal in the original data set from the apatitic mineral (factor B) at 50 μm and 140 μm through the transect than at 20 μm or 80 μm through the transect. Note that the collagen (factor A) and mineral (factor B) components are not colocalized throughout the tissue probed; hence, the FA separates these two tissue components into two separate factors. Differences in their scores indicate areas in the tissue where their relative amounts differ.

The FA results of the F15.5 specimens show one of the greatest advantages of FA—its signal-averaging effect. On visual examination of the Raman spectrum from the F15.5 specimen with the most mineral signal (Fig. 2, F15.5), there is no easily discernible carbonate band (CO_3^{2-} ν_1, 1065–1070 cm^{-1}). However, the FA shows that the apatitic mineral actually is carbonated (Fig. 3, factor B, CO_3^{2-} ν_1, 1066 cm^{-1}).

PN1 and PN3. At least two mineral environments were found in each of the transects in the PN1 and PN3 specimens. A set of mineral factors from a PN3 specimen with three resolvable mineral environments is shown in Fig. 4. The main mineral factor in all of the specimens was a carbonated apatitic mineral (PO_4^{3-} ν_1 ~956 cm^{-1}; Fig. 4, factor A). At least one additional resolvable mineral factor was present in all of transects; two additional mineral factors were resolvable in 33% and in 50% of the PN1 and PN3 specimens, respectively. A nonsubstituted, more crystalline apatitic lattice (962–964 cm^{-1})–resolvable factor was present more often then the disordered phosphate factor (945–950 cm^{-1}).

PN7 and PN14 and postnatal 6 months. In the PN7, PN14, and 6-month specimens, we were able to resolve only two separable mineral environments using FA; a set of mineral factors and scores from one of the PN14 transects is shown in Fig. 5. All spectra were dominated by the substituted phosphate mineral environment at ~956 cm^{-1} (with B-type carbonate present at ~1069 cm^{-1}; Fig. 5, factor A). A resolvable nonsubstituted apatitic band (~964 cm^{-1}; Fig. 5, factor B) was present also in three of the PN7 specimens, five of the PN14 specimens, and four of the 6-month-old specimens. However, in the presence of the more fully

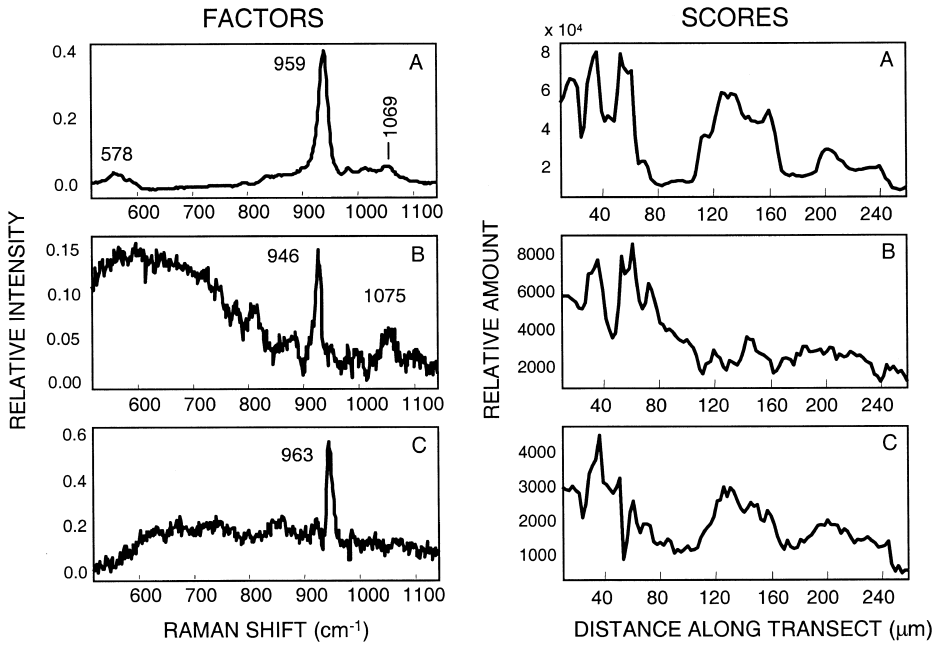

FIG. 4. FA reveals the presence of three resolvable mineral environments (959 cm^{-1}, 946 cm^{-1}, and 963 cm^{-1}) at PN3. Similar results were observed at PN1. For explanation of factors and scores and for experimental conditions see legend for Fig. 3. Factor A, carbonated apatite (PO_4^{3-} ν_1, 959 cm^{-1}; CO_3^{2-} ν_1, 1069 cm^{-1}); factor B disordered phosphate (PO_4^{3-} ν_1, 946 cm^{-1}); factor C, a more crystalline, nonsubstituted apatitic mineral (PO_4^{3-} ν_1, 963 cm^{-1}). Background factors have been omitted for clarity.

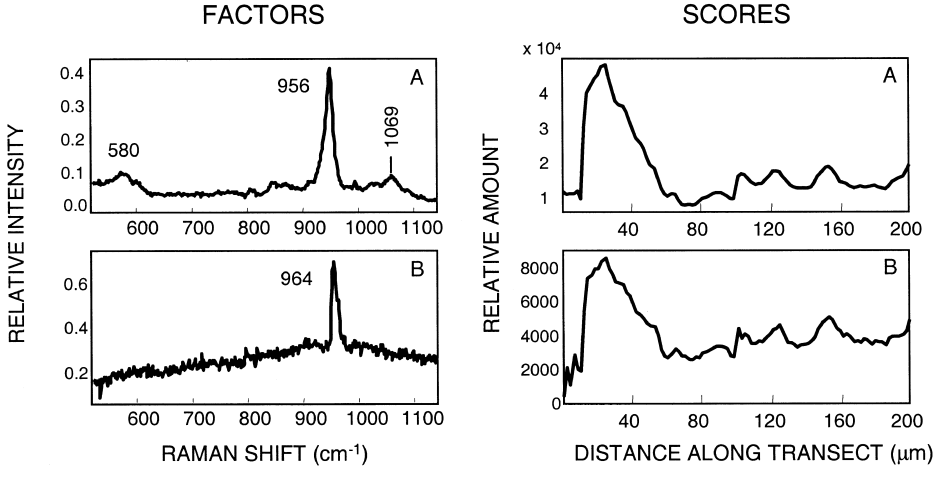

FIG. 5. Two resolvable mineral environments (956 cm^{-1} and 964 cm^{-1}) found in PN14; the resolvable disordered phosphate mineral environment is not present. Similar results were observed at PN7 and at 6 months. For explanation of factor and scores and for experimental conditions see legend for Fig. 3. Factor A, carbonated apatite (PO_4^{3-} ν_1, 956 cm^{-1}; CO_3^{2-} ν_1, 1069 cm^{-1}); B, a nonsubstituted apatitic mineral (PO_4^{3-} ν_1, 964 cm^{-1}). Background factors have been omitted for clarity.

mineralized tissue, the disordered phosphate factor (945–950 cm^{-1}) was separable in only one of the PN14 transects and was not found in any of the PN7 or 6-month-old specimens.

In the last two groups (the PN1 and PN3 group and the PN7, PN14, and 6-month group), more than one spatially resolvable mineral environment was present. The scores for the multiple mineral environments were different from one another (e.g., Fig. 4, in the 40- to 80- and 120- to 160-μm regions and Fig. 5 in the 40- to 60-μm region), but varied only a small amount—meaning that the mineral environments (lattice substitution and crystallite perfection) change only slightly throughout the distance of the tissue probed.

FA is especially useful in examining tissue in which the mineral deposition is incomplete. In the younger tissue (F15.5, F18.5, and PN1), the FA in all of the transects produced resolvable collagen and mineral factors, indicating that the mineralization was irregular and that the mineral was present in a different proportion than the collagen. (Fig. 3) As mineralization progresses, the mineral and collagen are not always resolved, meaning that the mineral is deposited evenly on the collagen matrix; in the PN3, PN7, and PN14 specimens, the mineral and collagen are resolved in one-half of the transects, and none are resolved in the 6-month-old mice. Hence, as the mouse ages and mineral deposition is more complete, the mineral is distributed evenly across the collagen over the distances and the spatial resolution of our measurements.

Univariate data analysis

Band area ratios: Carbonate/phosphate ratios. Although the FA of the F15.5 calvaria revealed the presence of a carbonate-substituted phosphate, the amount was so low

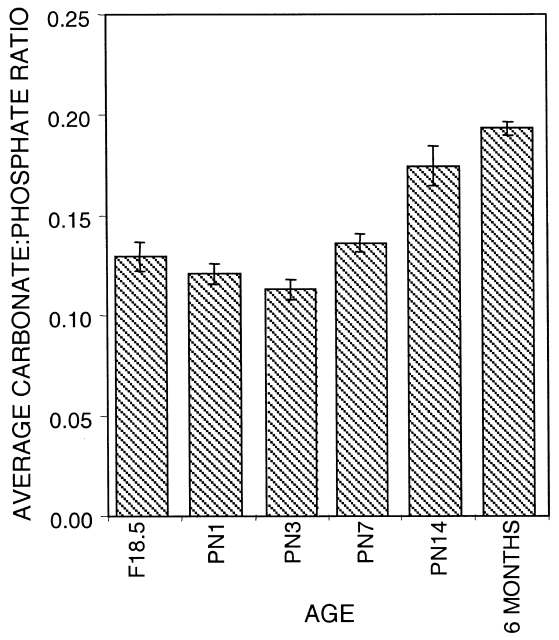

FIG. 6. Carbonate inclusion in the mineral lattice is constant from F18.5 to PN3 and then increases with age. Carbonate/phosphate band area ratios (CO_3^{2-} ν_1, 1070 cm^{-1}; PO_4^{3-} ν_1, 957 cm^{-1}) for F18.5 through 6-month-old specimens. The band area ratio is constant from F18.5 to PN3, and then increases with age. The values shown are the averaged carbonate/phosphate band area ratio for the six transects acquired for each age time point; the statistical uncertainties are equal to 1 SD. The carbonate/phosphate band area ratio for the F15.5 age specimen is not shown because the carbonate band intensity is too weak to allow an accurate band area calculation.

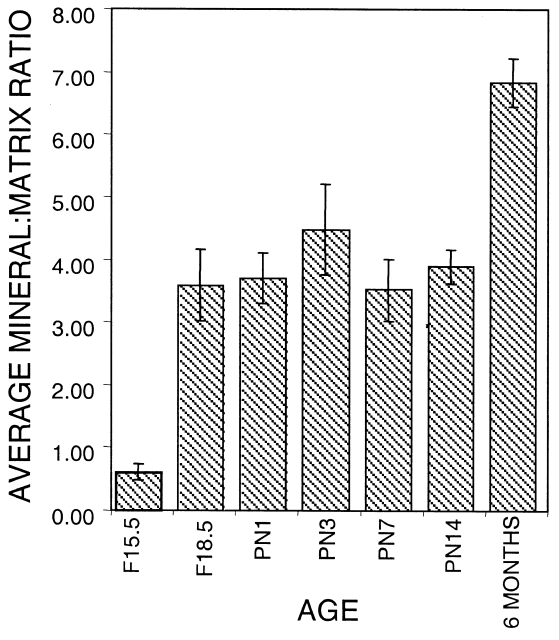

FIG. 7. Mineralization begins during fetal period, remains constant through early postnatal life and increases with age. Mineral/matrix band area ratios (PO_4^{3-} ν_1, 957 cm^{-1}; amide I, 1665 cm^{-1}) for F15.5 through 6-month-old specimens. The band area ratio increases from age F15.5 to F18.5, plateaus, and then increases again from the age of PN14 to 6 months old. The values shown are the averaged mineral/matrix band area ratio for the six transects acquired for each age time point; the statistical uncertainties are equal to 1 SD.

that the carbonate/phosphate ratios for F15.5 specimens could not be determined. In the rest of the specimens, the carbonate/phosphate ratio remained constant from F18.5 to PN3 and then increased with age (Fig. 6).

Band area ratios: Mineral/matrix ratios. The mineral/matrix ratio increases rapidly over the first 3 days of mineralization (F15.5–F18.5), reaches a plateau, and then increases between the ages of PN14 and the 6-month-old specimens (Fig. 7). The first and most significant increase in the mineral/matrix ratio is found between F15.5 and F18.5. During this period, mineral deposition is occurring rapidly and as a consequence, the mineral/matrix ratio drastically increases. The mineral/matrix ratios for the days of F18.5 through PN14 have reached a plateau, because the mineral/matrix ratio values over this age range are not different. However, it is evident that mineralization is not complete at PN14 because the mineral/matrix ratio is less than that of the 6-month-old specimens.

DISCUSSION

We have shown that Raman spectroscopy is a powerful technique to study mineralized tissues. Using both univariate and multivariate data analysis techniques, we were able to characterize the composition of the earliest mineral environment detected in the mouse calvaria and continue this characterization until a more mature mineral environment was formed. Using Raman spectroscopy, we have shown that the first appearance of mineral in mouse calvaria was observed at F15.5, consistent with alzarin red/Alcian blue staining studies,[4] and that this mineral is a carbonated apatite, similar to that observed by other initial mineralization studies of endochondral ossification[23,24] and cell cultures.[25,26] Although the mineralization of the F15.5 specimens was incomplete, mineral had certainly been deposited in several areas during the 24 h between E14.5 and F15.5. These data support previous studies that reported initial mineral deposition occurs at F15.5.[4] As mineralization progressed during the postnatal period, FA revealed the presence of more than one resolvable mineral factor, indicating that the tissue contained multiple mineral environments. The presence of multiple mineral environments is indicative of several mineralization processes occurring either simultaneously or sequentially.

We have shown that FA is a robust data analysis tool able to distinguish variations in Raman spectra (and hence in the original tissue components). In particular, FA enabled us to examine small variations in the mineral environment. Before discussing the relevance of each resolvable mineral environment, it is important to emphasize that the main mineral environment found throughout all of the tissue is a carbonated apatite. This substituted apatitic environment has varying levels of carbonate content throughout the de-

velopment of the mouse calvaria, but in all of the spectra in all of the tissue transects, this was the most prominent mineral environment observed. The other two resolvable mineral environments were a nonsubstituted, more crystalline apatite and a more disordered phosphate.

In the F15.5 and F18.5 calvaria, the carbonated apatite was the only mineral environment observed. This could be a result of the rapid deposition of a nearly homogeneous substituted, though not necessarily perfect, crystalline mineral. Another more likely possibility is that because there is less mineral, the signal to noise of the mineral vibrational bands is decreased. As a result of this decrease in signal to noise, small changes in the shoulders of the PO_4^{3-} ν_1 band throughout the transect are not resolved by the FA technique. As mineralization and growth continue after birth, it is possible that both osteoclastic resorption and remodeling of the previously deposited mineral as well as deposition of new mineral is occurring. If this mineral deposition and remodeling is occurring, it could be that the resulting mineral environment is not homogeneous. The appearance of more than one mineral factor in the older tissues is consistent with this interpretation.

Besides the most prominent factor (the carbonated apatite), FA revealed the presence of a resolvable nonsubstituted more crystalline apatite mineral factor in all of the postnatal time points, indicating that either a previously substituted mineral lattice is being remodeled (to remove substitutions and to perfect the lattice) or that a nonsubstituted apatitic phosphate lattice is being deposited. The more disordered phosphate environment, present in the PN1 and PN3 specimens, suggests that mineral maturation has not fully occurred and that osteoclastic resorption has not yet begun in these areas of the tissues. It could be that the disordered phosphate shoulder is no longer resolvable from the substituted apatitic phosphate in the PN7, PN14, and 6-month-old calvaria because remodeling is continuing and osteoclastic resorption is beginning, removing some of the disorder mineral from the lattice. The presence or absence of these two additional resolvable mineral factors helps illustrate the complexity of the early mineralization process.

We propose that carbonate/phosphate ratios that are constant (F18.5 to PN3) and then increase thereafter are a reflection of the concentration and availability of carbonate ions in the mineral environment. We believe that both through remodeling and new mineral deposition, any ions that are present in the mineral environment can be incorporated into the apatitic lattice. The work of Boskey et al. supports this hypothesis; using FTIR spectroscopy, they have shown that patients who have osteoporosis and are treated with sodium fluoride have increased mineral crystallite sizes in their tissue, indicative of fluoride ion incorporation.[27] We suggest then, that in the younger specimens, fewer carbonate ions may be available for incorporation into the mineral lattice. Birth may change the ionic equilibrium found in the tissue and may affect what ions are available for incorporation. The change in ions integrated into the mineral lattice after birth may not be measurable immediately; however, with the continuing, rapid calvarial mineralization, the change in ionic incorporation may become evident after PN3. As mineralization continues (growth, remodeling, and ionic incorporation after PN3), an increase in carbonation is observed with an increase in age. This is consistent with mineral maturation in fully mineralized tissue.

We found no evidence in the calvaria for thermodynamic precursors to apatitic mineral (dicalcium phosphate dihydrate, octacalcium phosphate, and amorphous calcium phosphate),[28] postulated to be precursors to biological apatite. It is interesting to note that no other vibrational spectroscopic studies of cell cultures and developing tissue have provided evidence for the proposed hydroxyapatite precursors.[1,3,23,25,26,29] It is possible that we did not detect these precursors because they were present only in small quantities and only for a few minutes or hours.

Raman microspectroscopy proved to be a valuable characterization tool in the study of early mineralized tissue. It offers several advantages over some more familiar bone tissue–characterization technologies such as FTIR, XRD, and electron microscopy (EM). Of these four technologies, Raman spectroscopy is the only nondestructive technique. Raman spectroscopy can be performed on in vitro and potentially on some in vivo specimens; hydrated specimens can be subjected to Raman spectroscopy because the O—H stretch does not obscure the tissue spectrum. Raman spectroscopy provides spatial information that XRD cannot because of the need to pulverize specimens before XRD analyses and Raman spectroscopy is capable of better spatial resolution (resolution down to 0.5 μm) than FTIR (10 μm). Raman spectroscopy also requires very little specimen preparation; the thin sections needed for FTIR analyses are not necessary for Raman analyses. Like FTIR spectroscopy, Raman spectroscopy also offers molecular speciation information that XRD and EM cannot. For example, Raman spectroscopy distinguishes a phosphorous atom in a hydroxyapatite lattice from a phosphorous atom in a phospholipid. In this work, we have been able to use Raman microspectroscopy to examine mouse calvaria and provide detailed compositional information about the tissue environment. We believe that Raman microspectroscopy also will prove useful in the study of birth defects affecting the skull, including the abnormal mineralization of the calvarial sutures in the disease craniosynostosis.

ACKNOWLEDGMENTS

The authors thank Jennifer Dreier (University of Michigan) for her assistance with specimen preparation and Dr. Jerilyn Timlin (Sandia National Laboratories), Dr. Jeremy Shaver (Eigenvector Research, Inc.), and Angela Carden (University of Michigan) for their helpful discussions regarding data analysis. This work was supported in part by the University of Michigan Center for Biomedical Engineering Research (to M.D.M.) and NIH/NIAMS 46024 (to M.D.M. and M.A.I. Jr.) and NIDCR grant DE 11530 (to M.A.I. Jr.).

REFERENCES

1. Stanford CM, Jacobson PA, Eanes ED, Lembke LA, Midura RJ 1995 Rapidly forming apatitic mineral in an osteoblastic cell line (UMR 106–01 BSP). J Biol Chem **270:**9420–9428.

2. Hoshi K, Ejiri S, Ozawa H 2001 Localization alterations of calcium, phosphorus, and calcification-related organics such as proteoglycans and alkaline phosphatase during bone calcification. J Bone Miner Res **16:**289–298.
3. Kuhn LT, Xu YT, Rey C, Gerstenfeld LC, Grynpas MD, Ackerman JL, Kim HM, Glimcher MJ 2000 Structure, composition, and maturation of newly deposited calcium-phosphate crystals in chicken osteoblast cell cultures. J Bone Miner Res **15:**1301–1309.
4. Johansen VA, Hall SH 1982 Morphogenesis of the mouse coronal suture. Acta Anat (Basel) **114:**58–67.
5. Carden A, Morris MD 2000 Application of vibrational spectroscopy to the study of mineralized tissues. J Biomed Opt **5:**259–268 (review).
6. Lawson EE, Barry BW, Williams AC, Edwards HGM 1997 Biomedical applications of Raman spectroscopy. J Raman Spectrosc **28:**111–117.
7. Kale S, Biermann S, Edwards C, Tarnowski C, Morris M, Long MW 2000 Three-dimensional cellular development is essential for ex vivo formation of human bone. Nat Biotechnol **18:**954–958.
8. Timlin JA, Carden A, Morris MD, Rajachar RM, Kohn DH 2000 Raman spectroscopic imaging markers for fatigue-related microdamage in bovine bone. Anal Chem **72:**2229–2236.
9. Timlin JA, Carden A, Morris MD 1999 Chemical microstructure of cortical bone probed by Raman transects. Appl Spectrosc **53:**1429–1435.
10. Timlin JA, Carden A, Morris MD, Bonadio JF, Hoffler CE, Kozloff KM, Goldstein SA 1999 Spatial distribution of phosphate species in mature and newly generated mammalian bone by hyperspectral Raman imaging. J Biomed Opt **4:**28–34.
11. Lin D-L, Tarnowski CP, Zhang J, Dai J, Rohn E, Patel AH, Morris MD, Keller ET 2001 Bone metastatic LNCaP-derivative C4–2B prostate cancer cell line mineralizes in vitro. Prostate **47:**212–221.
12. Penel G, Leroy G, Rey C, Bres E 1998 MicroRaman spectral study of the PO_4 and CO_3 vibrational modes in synthetic and biological apatites. Calcif Tissue Int **63:**475–481.
13. Kirchner MT, Edwards HGM, Lucy D, Pollard AM 1997 Ancient and modern specimens of human teeth: A Fourier transform Raman spectroscopic study. J Raman Spectrosc **28:**171–178.
14. Schrader B, ed. 1995 Infrared and Raman Spectroscopy: Methods and Applications. VCH Publishers, Inc., New York, NY, USA.
15. Chalmers JM, Everall NJ 1993 Vibrational spectroscopy. In: Hunt BJ, James MI (eds.) Polymer Characterisation. Blackie Academic & Professional, an imprint of Chapman & Hall, Bishopbriggs, Glasgow, Scotland, pp. 69–114.
16. de Grauw CJ, de Bruijn JD, Otto C, Greve J 1996 Investigation of bone and calcium phosphate coatings and crystallinity determination using Raman microspectroscopy. Cell Mater **6:**57–62.
17. Geladi P, Grahn H 1996 Multivariate Image Analysis. John Wiley & Sons Ltd., West Sussex, UK.
18. Reyment R, Jöreskog KG 1996 Applied Factor Analysis in the Natural Sciences, 2nd ed. Cambridge University Press, Cambridge, UK.
19. Adams MJ, 1995 Chemometrics in Analytical Spectroscopy. The Royal Society of Chemistry, Cambridge, UK.
20. Otto M, 1999 Chemometrics: Statistics and Computer Application in Analytical Chemistry. Wiley-VCH, New York, NY, USA.
21. Jestel NL, Shaver JM, Morris MD 1998 Hyperspectral Raman line imaging on an aluminosilicate glass. Appl Spectrosc **52:**64–69.
22. Camacho NP, Rinnerthaler S, Paschalis EP, Mendelsohn R, Boskey AL, Fratzl P 1999 Complementary information on bone ultrastructure from scanning small angle X-ray scattering and Fourier-transform infrared microspectroscopy. Bone **25:**287–293.
23. Mendelsohn R, Jassankhani A, DiCarlo E, Boskey A 1989 FT-IR microscopy of endochondral ossification at 20 μm spatial resolution. Calcif Tissue Int **44:**20–24.
24. Rey C, Hina A, Tofighi A, Glimcher MJ 1995 Maturation of poorly crystalline apatites: Chemical and structural aspects in vivo and in vitro. Cell Mater **5:**345–356.
25. Rey C, Kim H-M, Gerstenfeld L, Glimcher MJ 1996 Characterization of the apatite crystals of bone and their maturation in osteoblast cell culture: Comparison with native bone crystals. Connect Tissue Res **34:**343–349, 397–403.
26. Rey C, Kim H-M, Gerstenfeld L, Glimcher MJ 1995 Structural and chemical characteristics and maturation of the calcium-phosphate crystals formed during the calcification of the organic matrix synthesized by chicken osteoblasts in cell culture. J Bone Miner Res **10:**1577–1588.
27. Boskey AL 1990 Bone mineral and matrix: Are they altered in osteoporosis? Orthop Clin North Am **21:**19–29.
28. Nancollas GH, Lore M, Perez L, Richardson C, Zawacki SJ 1989 Mineral phases of calcium phosphate. Anat Rec **224:**234–241.
29. Boskey AL, Pleshko Camacho N, Mendelsohn R, Doty SB, Binderman I 1992 FT-IR microscopic mappings of early mineralization in chick limb bud mesenchymal cell cultures. Calcif Tissue Int **51:**443–448.

Address reprint requests to:
Michael A. Ignelzi, Jr., D.D.S., Ph.D.
Department of Orthodontics and Pediatric Dentistry
The University of Michigan School of Dentistry
1011 North University Avenue
W. K. Kellogg Building, Room 2532
Ann Arbor, Michigan 48109-1078, USA

Received in original form May 21, 2001; in revised form January 7, 2002; accepted January 22, 2002.